Wearable Multiple Modality Bio-signal Recording and Processing on Chip: A Review

Qiuyang Lin, *Student Member*, *IEEE*, Shuang Song, *Member*, *IEEE*, Ivan D. Castro, Hui Jiang, *Member*, *IEEE*, Mario Konijnenburg, *Member*, *IEEE,* Roland van Wegberg, Dwaipayan Biswas, *Member*, *IEEE*, Stefano Stanzione, *Member*, *IEEE*, Wim Sijbers, Chris van Hoof, *Member*, *IEEE*, Filip Tavernier, *Member, IEEE,* Nick van Helleputte, *Member*, *IEEE*

***Abstract*— Remote home monitoring via wearables is rapidly gaining popularity, thanks to ever more complex vital signs recording and data analytics that are embedded into single devices. True system-on-chips (SoCs) push the envelope of power and form factor, while wearables are becoming more common-place, novel health sensing paradigms appear. Non-contact sensing technologies enable vital signs sensing without requiring any physical contact with the human body. This paper reviews existing multiple-modality bio-signal recording and processing SoCs, circuit techniques for individual bio-signal readout channels including electrocardiography (ECG), Electroencephalography (EEG), Bio-impedance (BioZ), photoplethysmography (PPG), and non-contact sensing with high user comfort. The state-of-the-art wearable sensor interfaces and systems together with future development trends are provided.**

***Index Terms*— Bio-signal recording, low-power, SoCs, ECG, EEG, BioZ, PPG, non-contact monitoring.**

I. Introduction

Wearable healthcare devices like smartwatches and patches are becoming increasingly prevalent because they foster the shift of healthcare from curing patients to monitoring and improving health condition of people who did not develop a disease yet. Various biopotential signals and bio-current signals can be used to extract vital signs for health monitoring applications, as shown in Fig. 1. i.e. electrocardiography (ECG) can provide heart rate (HR), heart rate variability (HRV), photoplethysmography (PPG) can provide oxygen saturation (SpO_2) and together with ECG, blood pressure can be extracted [1]-[4]. These physiological parameters can be used for diagnostics of cardiovascular disease, which counts for around one-third of total deaths worldwide [5]. Electroencephalogram (EEG) and near infrared spectroscopy (NIRS) can be used for brain monitoring, indicating the anesthesia depth during the surgery and bio-impedance (BioZ) recordings can be used to monitor respiratory diseases and analyze body composition for general fitness, but also for renal failure or chronic heart [6]-[11].

Manuscript submitted February 15, 2020, revised June 21 and August 2, 2020, accepted August 9, 2020. The associate editor coordinating the review of this article and approving it for publication was Dr. Zhichao Tan (Corresponding author: Shuang Song)

Q. Lin, S. Song, I. D. Castro, W. Sijbers, D. Biswas, C. Van Hoof and N. Van Helleputte are with imec, Heverlee, 3001, Belgium (e-mail: shuang.song@imec.be; nick.vanhelleputte@imec.be).

Q. Lin, C. Van Hoof and F. Tavernier are also with the Department of Electrical Engineering (ESAT), KU Leuven, Leuven, 3000, Belgium (email: Filip.Tavernier@esat.kuleuven.be; chris.vanhoof@imec.be)

H. Jiang, M. Konijnenburg, R. van Wegberg, S. Stanzione, are with the Holst Centre/imec, Eindhoven 5656AE, The Netherlands (e-mail: roland.vanweberg@imec.nl; mario.konijnenburg@imec.nl)

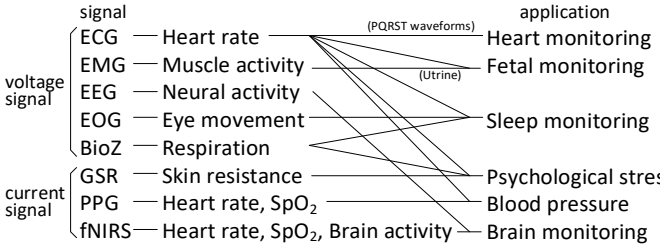

Fig. 1. Multiple physiological-signal and possible applications

Multiple modality bio-signal recording and processing SoCs have been therefore developed in recent years as the core of wearable devices [12]-[17].

Integrating multiple modality sensing channels including ECG, BioZ, galvanic-skin response (GSR), PPG/NIRS, etc. together with power management and other auxiliary circuitry in a monolithic SoC can reduce the size, cost and complexity of monitoring system, resulting in good user comfort and wide application range [18]-[20]. Moreover, microprocessors (MCUs) that enable edge computing to extract on-chip physiological parameters like HR, HRV, respiration ratio (RR) and SpO_2 are included in the SoC together with certain hardware accelerators and memory. Wired and wireless data interfaces like serial peripheral interface (SPI), universal serial bus (USB) and Bluetooth low energy (BLE) radio and power management unit are also integrated. To obtain multiple bio-signals with medical-grade quality with low-power consumption (mW level) is the major system-level design challenge for wearable recording and processing SoCs.

Regarding the readout channels, each bio-signal has different requirements on the readout frontend. The ECG readout

frontend has been studied intensively in past decades. The major challenge is dealing with the large electrode offset while maintaining a high input impedance and a low noise level. For some special applications, i.e. in fetal ECG monitoring, a multiple-channel readout with a very low-noise level is required [21]. For BioZ readouts, achieving a low input-referred impedance noise density is of paramount importance to recognize small BioZ variation representing the heartbeat and respiration. A high dynamic range (DR) readout for PPG/NIRS application is needed to extract the small hemodynamic (AC) response in the presence of the large baseline (DC) component.

To prolong the battery lifetime, the system power consumption should be minimized. The power consumption of a typical multiple modality bio-signal recording SoC is dominated by the MCU when the physiological parameter extraction algorithm is running. This power decreases significantly with technology node as shown in [12][22]. From analog circuitry point of view, the power consumption is dominated by the LED drivers for generating the PPG/NIRS signal. This can be solved by using duty-cycled LEDs or more efficient photodetector, i.e. silicon photomultiplier or monolithic photodiode (PD) [23]-[26].

While existing wearable devices clearly advance hospital - based healthcare monitoring systems in terms of form factor, user comfort and power consumption, a further step is embedding healthcare monitoring into daily life. In the last couple of decades, several technologies have been developed for bio-signal recording with unobtrusive sensors integrated into users' daily life. To give one example, Non-contact ECG/BioZ acquired through clothing in a capacitively-coupled manner can provide a more attractive solution because the devices can be embedded in chairs, beds or clothing. Compared with wearable ECG and BioZ monitoring, this technique does not require sticky wet electrodes neither skin preparation, which is not user-friendly during long-term monitoring. However, it also poses several strict requirements on the readout circuit. e.g. the input impedance should be ultra-high (>10G) and the common-mode input range and the common-mode rejection ratio (CMRR) should also be higher than those for conventional ECG readout.

The rest of this paper is organized as follows: Section II reviews the system architecture of the state-of-the-art highly integrated SoCs for multi-modality bio-signal sensing. Section III covers the high-performance electrical sensing modalities including ExG and BioZ sensing. Section IV presents the latest optical sensing modalities, i.e. PPG and NIRS readout circuitry. Section V gives an overview of recent developments in non-contact capacitively-coupled sensing technology while conclusions are drawn in section VI.

II. System Architecture

A very small form factor while maintaining excellent signal quality and reliability is critical for wearable devices for medical purposes. On the system level, a high degree of integration and a low power consumption help to reduce the system form factor by reducing the number of off-chip components and the battery size. Subsection A and B focus on these two aspects, respectively.

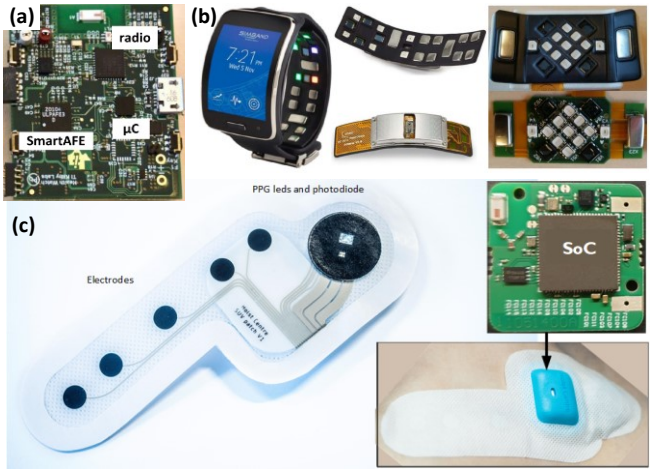

Fig. 2. (a) The System on PCB using the AFE SoC in [14], (b) The smartwatch and its PCB using the SoC and PMIC in [13] and (c) The health-patch and its PCB using the SoC in [16]

A. Overview of SoCs for bio-signal acquisition

Several multiple sensing SoC solutions for wearable devices have been developed in recent years [12]-[17]. In [12], a 345µW ECG/Electrode-tissue impedance (ETI)/BioZ recording SoC with the digital signal processor (DSP) and accelerators integrated. It was the first time an ECG recording channel including ETI based real-time motion artifact (MA) estimation and cancellation algorithm running on the same chip, although it was found out later that the correlation between the ETI and MA signal was not perfect. This work is the first attempt to integrate several sensing modalities, but it still requires several discrete power management circuitry chips i.e. switched-mode power supply (SMPS)/low dropout regulator (LDO) to complete a battery power system. Konijnenburg et al. [13] proposed a recording SoC for concurrent ECG, BioZ, GSR, and PPG including the LED drivers and a similar DSP as [12]. Under the same framework [13], a separate power management IC (PMIC) specified for multiple modality devices including a complete set of SMPSs and LDOs was also proposed to avoid possible power line interference from the PMIC to the readout SoC. The SoC and PMIC can be considered as a further step towards a miniature wearable system. Schönle et al. [16] reported an SoC including 9 channels of reconfigurable ExG (ECG/EEG/EMG) and 4 channels of PPG, 6 channels of neural stimulation (NS), 1 channel of temperature sensing (TS) with PMIC and micro processing unit (PMU) integrated with the readout channels. Shu et al. recently presented a recording SoC including ECG BioZ and PPG recording channels, where several techniques are proposed to enhance the DR of PPG channel and enable two-electrode monitoring of ECG [15].

The level of integration achieved by the aforementioned solutions are still limited because: 1) the data interface is still based on wired connection e.g. SPI/USB; 2) the DSP has relatively low processing ability. The main reason for the limited integration level is the conventional technology node ([13][16]), which is chosen for the analog frontend. Indeed,

Table I: Comparison of system architectures of exiting multiple modality bio-signal recoding and processing SoCs

	[13]	[14]	[15]	[16]	[17]
Technology (nm)	180	130	55	130	55
Type	SoC	MCM	SoC	SoC	SoC
Area (mm^2)	37.7	1360	4.5	20.8	18.49
V_{DDAFE} (V)	1.2	1.5	1.8/2.8	1.5	1.2
V_{DDDig} (V)	1.2	0.6	0.9	0.6-1.2	0.6 - 1.2
Analogue block	ECG/BioZ/PPG /GSR/PMIC/LED drivers	ECG/PPG /LED driver	ECG/BioZ/PPG /GSR/LED drivers	EXG/PPG/BioZ/PMIC /NS/TS/LED driver	ECG/BioZ/PPG /PMIC/LED drivers
MCU	ARM M0	MSP 430	-	PULP	ARM M4f
SRAM (kB)	128	-	16	128+32	192
Accelerators	DMA, Maxtrix, Sample Rate Converter	-	FIR/IIR, DDS, BioZ, CORDIC, DC	-	DMA, FFT, Maxtrix, Sample Rate Converter
Data interfaces	SPI/UART/I2C	BLE radio	SPI/I2C	SPI/UART/I2C/JTAG/GPIO	BLE/USB/SPI/UART/I2C
Security	No	No	No	No	Yes

analog frontends do not benefit from a more advanced node because of the bandwidth of interest is low, however on-chip digital processing and wireless data communication can be implemented with higher area and power efficiency [17].

An all-in-one battery-powered SoC implemented in a 55nm technology node is proposed in [27] for low-cost single-use health patches. The integration of MCU, Bluetooth and digital signal processing accelerators together with multiple modality readout frontends (ECG, BIOZ and PPG) significantly reduces the number of off-chip components. As shown in Fig.2 (a), due to a low level of integration, the readout SoC in [14] needs many off-chip components on PCB. The smartwatch PCB using the SoC and PMIC in [13] and the health patch PCB using the all-in-one SoC [16] are shown in Fig. 2 (b) and (c), respectively. It can be seen in Fig. 2 (c) that, much less components around the SoC are needed, which include the antenna, matching circuits, crystals, (decoupling) capacitances and safety resistors. The off-PCB components include the electrodes, two LEDs, and photodiodes integrated in the flexible patch.

Instead of all-in-one SoC, implementing analog/digital IPs in different process nodes and integrating them, e.g. 3-D vertical integration, system-in-package (SiP) solutions, and package-on -package, provide another interesting possibility. Implementing analog/digital/wireless IPs at their own optimal process could provide a lower total chip cost and provide higher performance of individual circuit blocks; one example can be found in [28]. However, for SiP solutions, the complexity of multiple modality recoding and processing requires hundreds of bonding wires between analog, digital and wireless IPs, leading to reliability issues. Moreover, software tools for design and verification of 3-D/package integration are not as mature as tools for IC chips, giving another degree of risk, e. g. noise coupling through silicon vias between different dies [29]. Therefore, all-in-one SoCs remain the best solution for multiple modality bio-signal recording and processing according to the current state-of-the-art.

B. Power consumption and edge computing

The power consumption of bio-signal acoustician and processing SoCs is of paramount importance for long time monitoring and user comfort with a small battery. The total power consumption typically consists four important parts: 1) the analog readout channels that consume around several hundreds of μW, depending on the number of modalities and channel; 2) the LEDs for PPG/NIRS excitation that consume several hundreds of μW to several mW, depending on measurement locations and factors like skin color etc; 3) the MCU together with clock generation and memory that consumes usually several hundreds of μW for philological parameters extraction; and 4) the radio that can consume several tens of μW up to several mW, depending on the data rate [16][17]. Among these four parts, the power of the analog readout channels and the LEDs (included in the optical readout channel) is determined by the required signal quality (SNR), which will be discussed in section III and IV, respectively.

Considering the power consumption of digital processing and the ratio, the required data processing and physiological parameter extraction can be executed in two ways: 1) the raw measurement data is sent via radio to a central node, which processes the signal; 2) the raw data is processed at the multiple sensor SoC and only the extracted information is sent. This is a fundamental design choice which determines the system deployment and the total power consumption. While a comprehensive comparison between the data processing power and radio power is very difficult because of the different data rates and complexity of the algorithm, an example based on 3 channel ECG data (12bit, 512sps) with typical instantaneous heart rate extraction is discussed.

$$P = \frac{1}{2} \cdot CV_{supply}^2 \quad (1)$$

To the best of our knowledge, an energy efficiency of around 1nJ/bit can be assumed for BLE radios [30][31], both implemented in 40nm CMOS technology, resulting in a power of around 20μW to transmit 3 typical ECG traces. On the other hand, similar power numbers (~10μW) are reported in [32][33] for HR extraction, implemented in 90nm technology, respectively. With continuous scaling down of technology node, the active power of data processing will shrink much faster than the radio power as shown in Eq. 1, because the power reduction for the radio (assuming the same architecture) is mainly from the reduction of supply voltage. Besides, an SoC implemented in 0.13μm technology is shown in [34] where a total power of

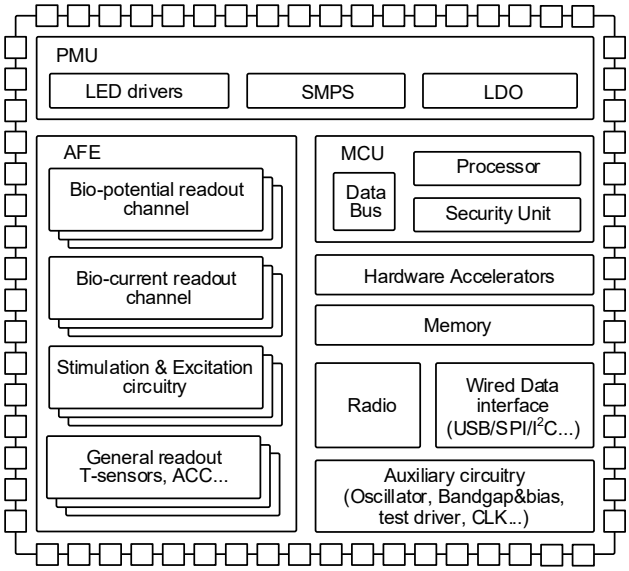

Fig. 3. System schematic of an ideal multiple modality SoC

17.4μW is reported for recoding 2 channels of ECG and on-body extracting of the heart rate, while a power of 74.8μW is required for sending the raw data. Another solution implemented also in 0.13μm [16] reports 620μW digital processing power for extracting heart rate, pulse wave velocity (PWV) and blood pressure from channels of PPG (10kHz, 16bit), while 26mW is needed for sending the raw data.

It is evident from the above-mentioned literature that processing the data on the sensor platform (i.e. edge computing), helps achieve energy efficiency as compared to continuous transmission of raw data. Processing the data on the edge is achieved through dedicated low-power accelerators, extending the life of battery-powered sensor nodes and enabling long-term continuous/real-time monitoring. With the fast development of machine learning technology, this approach is commonly adopted for executing the real-time inference of trained model parameters on sensor data, while the compute-intensive training is performed off-line [35]. The computational complexity of inference is much less than conventional signal processing algorithms, reducing the required hardware resource, power consumption and system form factor.

Apart from battery powered SoCs, energy harvesting and wireless powering-based solutions also have been proposed. A battery-less SoC with 4-channel ExG is proposed in [36], which includes a thermoelectric generator (TEG) with a boost converter and a RF kick-start circuit. In an R-R interval detection mode, the whole SoC consumes a power of 19μW, where the MCU extracts the interval on chip and the radio sends data every 5 seconds. This solution is another good example of power minimization by on-body data processing before sending. The SiP solution [28] mentioned already in subsection A also exploits energy harvesting from TEG and solar component, consuming a total power of 6μW when recording and sending one channel of raw ECG sampled at 100sps. While energy harvesting based solutions may suffer from an unstable power flow, wireless powered SoCs have been proposed to support a more reliable continuous operation [37][38][39]. Wireless powering with additional inductance or capacitive components has its advantage in implantable application like electrocorticography (ECoG), where changing the battery is difficult. However, for wearable ambulatory monitoring with mW level power, the most reliable and efficient way of powering remains to be the battery, though energy harvesting and wireless powering may work as secondary power sources to extend the battery lifetime.

Hereby, the system schematic of an ideal multiple modality bio-SoC is shown in Fig. 3 including all the required functional blocks. Table I compares the state-of-the-arts multiple modality bio-signal recoding and processing SoCs.

III. Electrical Readout Channel

Biopotential and bioimpedance signals are the main bioelectrical signals. Among biopotential signals, ECG and EEG are the most prevalent recording modalities, where the ECG enables HR/HRV extraction as well as morphology analysis and EEG provides insight into brain activities. Meanwhile, the bio-impedance (BioZ) channel enables respiration rate extraction by measuring the impedance of human tissue. The ECG, EEG and the BioZ readout channel are reviewed in subsection A, B and C, respectively.

A. ECG readout channel

The first sub-100μW ECG readout channel for wearable devices was proposed in [40], and similar works can be found later in [12]. The research has been focused on achieving a low noise level at minimal power, while other performance parameters like input impedance, CMRR and PSRR should be sufficiently high. Also, the electrode offset should be compensated to avoid saturation. The noise-power performance of different readout amplifiers can be compared with the noise efficiency factor (*NEF*), which is defined in Eq. 2 [41]. The NEF describes how many times the noise of a system with the same current and bandwidth is higher compared to that of an ideal bipolar transistor.

$$NEF = V_{rms}\sqrt{\frac{2I_{tot}}{\pi \cdot V_t \cdot 4kT \cdot BW}} \quad (2)$$

With the widespread of current-reuse technique, the NEF has been reduced continuously in the past two decades [21][40][42][43]. Nevertheless, from a system point of view, further reducing the power consumption of an ECG amplifier below 1μW does not have any significant impact. Furthermore, it is important to realize that the NEF only takes power, noise and BW into account, parameters like input impedance, CMRR, DC offset rejection, input range, linearity, etc. are all important and often consumes more power and area than noise/BW constraints [12]. For example, chopping technique reduces the 1/*f* noise and improves CMRR, while it degrades the input impedance and poses a higher requirement for IA's bandwidth [12][21]. Therefore, additional power may be needed for an active bootstrap circuit to boost the input impedance and sometimes for a ripple reduction loop to suppress the up-modulated amplifier DC offset [45], which helps to increase the input range. Also because of chopping, the HPF used to reject

This article has been accepted for publication in a future issue of this journal, but has not been fully edited. Content may change prior to final publication. Citation information: DOI 10.1109/JSEN.2020.3016115, IEEE Sensors Journal

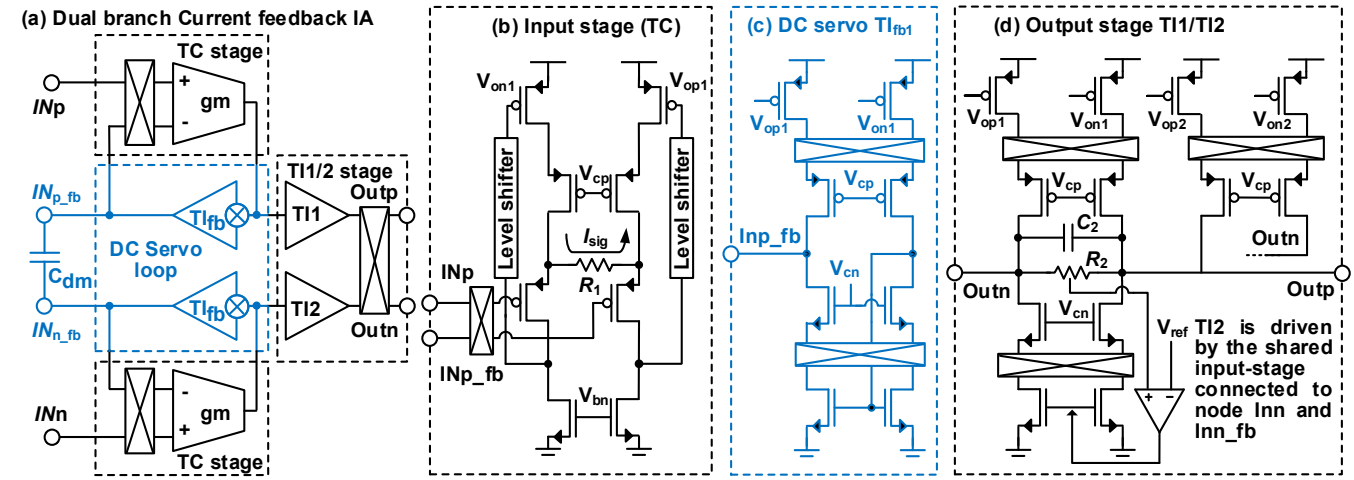

Fig. 4. Dual-branch current feedback readout amplifier topology

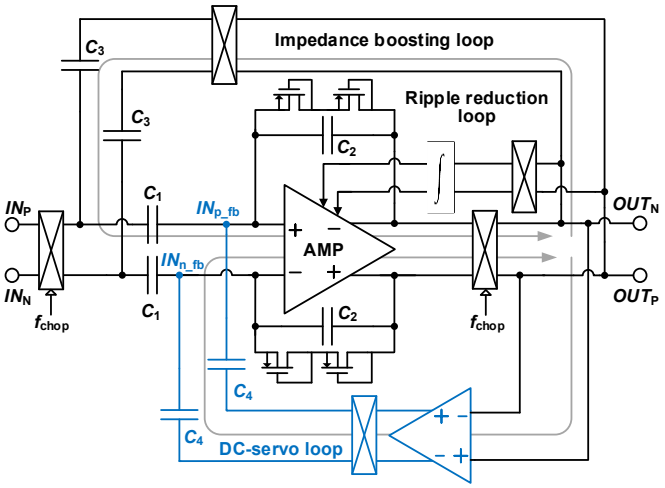

Fig. 5. Multiple-loop capacitive feedback readout amplifier topology

electrode DC offset has to be implemented by an active DC-servo loop, increasing the power. From area point of view, large components are needed for the low cut-off frequency of the HPF [12][35]. Pseudo resistors can be used with small area but they lead to leakage current and PVT problem [44]. Two typical ECG amplifier topologies (current feedback and capacitive feedback) with a good trade-off between noise, power, CMRR, PSRR and offset cancellation are discussed below.

As shown in Fig. 4 the dual-branch current feedback amplifier proposed in [12] exploits the large common-mode input range of two separated transconductance (TC) and half DC-servo stages (Fig. 4 (a)) for the positive and negative input nodes, generating a copy of electrode DC offset on C_{dm} capacitor. As the result, more than 200mV offset rejection is provided. Meanwhile, this topology achieves state-of-the-art CMRR, PSRR and input impedance performances at the cost of relatively high power consumption. This high power consumption is due to 1) the dual-branch configuration and 2) the current needed to compensate for the additional noise from the source degeneration resistor R_1 shown in Fig.4 (b).

Alternatively, a multiple-loop capacitive feedback topology proposed in [45][46] (Fig. 5) consumes only around 10% of the aforementioned current feedback topology while achieving almost the same input noise density, because capacitors do not

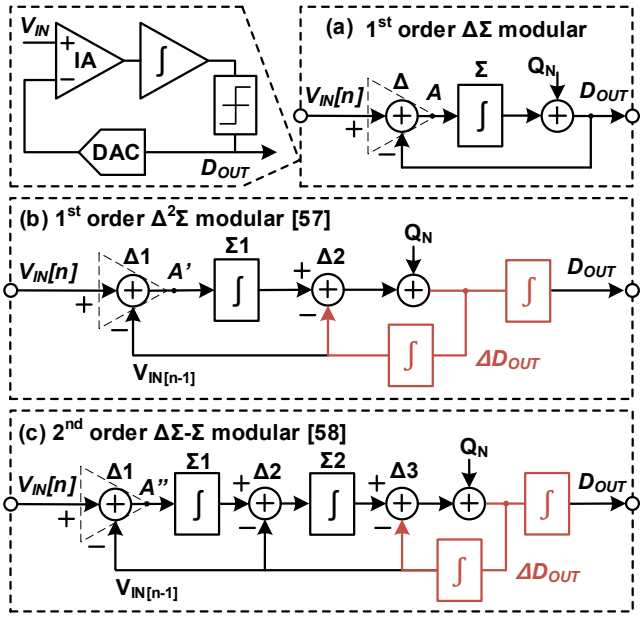

Fig. 6. Direction conversion with IA embedded (a) 1st order ΔΣ modulator (b) 1st order $\Delta^2\Sigma$ modulator [57]. (c) 2nd order ΔΣ-Σ modulator [58]

contribute additional noise. The chopper-stabilization scheme is applied to reduce the 1/*f* noise while increasing CMRR and PSRR. However, as shown in Fig. 5, the input capacitors operate at the chopping frequency, which results in low input impedance. A positive feedback loop can be used to boost the input impedance, but in practical implementations, the achieved impedance is only 10% of the one achieved in [12] due to a trade-off with loop instability as discussed in [47][48]. In addition, a DC-servo loop is applied to cancel the electrode DC offset and a ripple-reduction loop is used to cancel the amplifier input offset. Several ECG readout SoCs with wireless data link/power transfer employ capacitive feedback topology [37][49][50]. In both solutions, the chopping scheme, the DC-servo and impedance boosting loops are not implemented to minimize the power consumption.

B. EEG readout channel

The EEG readout has similar specifications in noise /bandwidth, and therefore, similar design challenges involving trade-off between noise, power, offset tolerance, input

Table III ECG/ExG Performance comparison table

	[12]	[62]	[45]	[54]	[55]	[46]	[56]	[58]	[59]	[60]
Technology	180nm	55nm	65nm	130nm	350nm	40nm	65nm	130nm	180nm	65nm
Supply (V)	1.2	1.2	1.0	1.2/3.3	2.5	1.2	0.5	1.2/3.3	1.8	0.8
Topology	Current feedback	Current feedback	Cap. feedback	Current feedback	Cap. feedback	Cap. feedback	Digital DC-servo	Direct Conversion	Direct Conversion	Direct Conversion
Area(mm^2)	-	4[1]	0.1	2.19[2]	0.12	0.069	0.013	0.013	0.48	0.024
Z_{in} (Ω)	1G	680M	30M	235M	-	1.6G	>30G	>100M	34M	>26M
Input Noise (μVrms in Hz)	0.61 0.5-150	0.47 0.5-150	1.3 0.1-500	0.8 1-100	2.81 0.5-1000	1.8 1-200	4.3 300	1.13 0.1-500	0.98 100	0.99 500
CMRR (dB)	110	98	134	101	82	-	75	-	109	81
Power (μW)	56	43	1.8	-	0.8	2.8	5	0.63	73.8[3]	0.8

[1]4 channels [2]8 channels [3]reference generation & test buffers included

impedance and CMRR, which is discussed in a comprehensive review work [51]. Several readout amplifiers for general bio-potential (ExG) signals are proposed [52]-[55], providing high user flexibility. As discussed in [51], conventional EEG readout solutions employ an analog DC servo-loop to cancel the electrode offset, requiring large components for the low corner frequency. A mixed-signal implementation of the DC servo-loop can reduce the chip area effectively as reported in [56]. In recent years, a direct to digital conversion scheme is proposed for neural recording and EEG readout applications. This scheme merges the amplification and quantization into a single stage, resulting in a compact architecture, a reduced chip area and a low cost [57]-[60].

As shown in Fig.6 (a), a ΔΣ style direction conversion scheme with IA embedded is considered in [58], where a reconstructed input is feedback and subtracted from the input, cancelling the DC offset before integration, however, due to the high gain of the IA, the residue at node *A* can still saturate the integrator and the quantizer. A discrete time $\Delta^2\Sigma$ scheme is then proposed by splitting the integration to both the forward path and feedback path, generating a copy of the input *x*[n-1]. Thus, the signal at node *A'* in Fig. 6(b) becomes the difference between two discrete time samples, avoiding saturation of the quantizer. The first work with this scheme reports a 5X reduction in chip area while achieving comparable performance [58].

Several other implementations of this concept have been reported. Yang et al. proposed in [59] a second-order ΔΣ-Σ (Fig. 6(c)) modulator to reduce the required OSR with the same noise shaping effect, providing 300 mV DC offset rejection. C. Kim proposed in [60] a mixed signal mode DC-servo loop to cancel the DC offset before it enters the first order ΔΣ modulator that merges the IA and ADC. Last but not the least, VCO based solutions [61] are also reported with significant chip area reduction. A benchmarking including recent ECG/EEG work is given in table III.

C. BioZ readout channel

Different from ECG readout channels, to monitor the body impedance variation with a mΩ-level resolution, a BioZ readout channel requires anxcitation, which is often in the current domain (Fig. 7 (a)) [63]. Consequently, the noise performance is not only determined by the readout front-end, usually an IA followed by an ADC, but also the current excitation circuit (CG) [12]. In conventional four-electrode BioZ readout channel

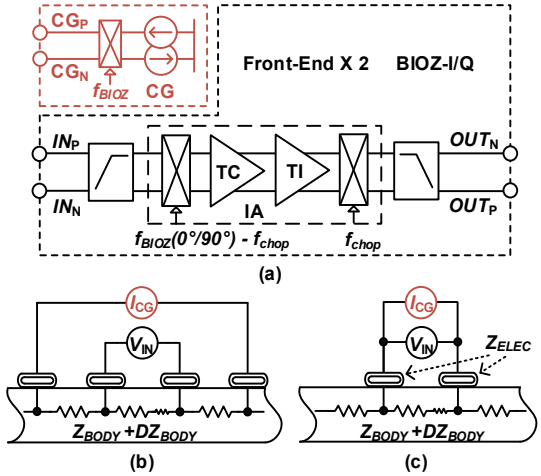

Fig. 7. Bio-Impedance Readout Channel (a) Bio-impedance measurement setup and comparison between (b) 4- and (c) 2-electrode configuration

(Fig. 7 (b)), the noise contribution due to the current generation circuits is to some extent relaxed by the relatively small body impedance (ZBODY < 100 Ω):

$$\overline{v_{N.BioZ}}^2 = \overline{v_{N.IA}}^2 + \left(\overline{i_{N.CG}}^2 + \overline{i_{N.REF}}^2\right) \times Z_{BODY}{}^2 \quad (3)$$

where $v_{N.BioZ}$, $v_{N.IA}$, are the noise of the BioZ channel and the IA, referred to the input of the IA; $i_{N.CG}$ and $i_{N.REF}$ the noise of the CG and its reference. Therefore, considerable efforts had been made to improve the energy efficiency of the IA [10] [12][13][16][64][65].

Alternatively, a two-electrode BioZ readout method (Fig. 7 (c)) could be a more promising candidate in the cost and size constrained applications, such as patches [27] and smartwatches [13], due to the halved number of electrodes. However, as the electrode impedance will also be processed, the current noise of the CG will start to dominate the noise performance of the BioZ readout channel, given by:

$$\overline{v_{N.BioZ}}^2 = \overline{v_{N.IA}}^2 + \left(\overline{i_{N.CG}}^2 + \overline{i_{N.REF}}^2\right) \times (2 \cdot Z_{ELEC} + Z_{BODY})^2 \quad (4)$$

where Z_{ELEC} is often in a range of 500 Ω to 2 kΩ. Even worse, the requirement for the input dynamic range is increased from ~10 mV to ~100 mV, which usually leads to an IA with a smaller gain and the following ADC with lower noise. Both of which degrade the energy efficiency of the BioZ readout channel.

To meet this challenge, a digital-assisted baseline cancellation scheme is proposed [66]. As shown in Fig. 8 (a), IDAC, controlled by the code that is extracted from the digital output of the ADC and biased by I_{REF}, which is the same as CG,

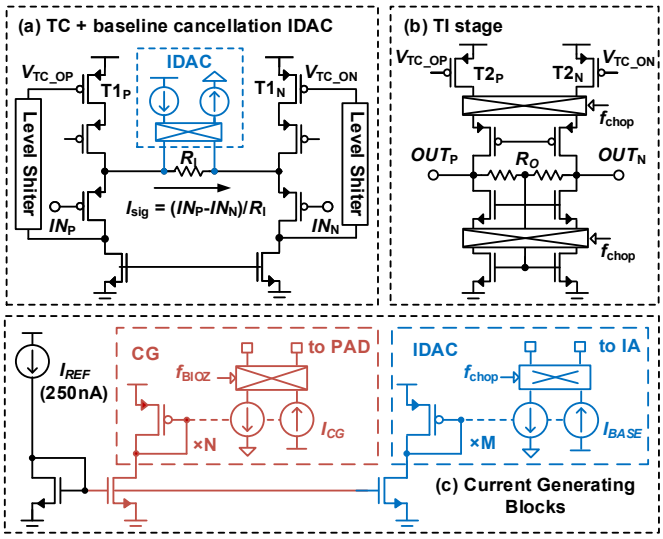

Fig. 8. (a)(b) Baseline cancellation in current domain and (c) resulting correlated noise cancellation. TC (transconductance), TI (transimpedance)

Table IV BioZ Performance comparison table

		[66]	[65]	[17]	[10]
Technology		55nm	65nm	130nm	180
Area (mm^2)		0.74	4.83	0.96	0.88
Supply		1.2	0.5	1.5/3.5	1.2/1.8
Input range (Ω)		24k	600	10k	1k
Resolution (mΩ/√Hz)		0.4 (40Ω) 7.0 (2kΩ)	15.28 (100Ω)	0.7 (<50Ω) 95 (2kΩ)	1.1 (20Ω) 26.0 (1kΩ)
Power (μW)	AFE	31-155	9.26	89[2]	18.7
	CG	19-35[1]		56-95	54-229

[1]1 channel only [2]w/o ADC

is used to compensate the large DC component of the I_{TC}, as shown in Fig. 8(a)(b). The smaller effective signal can be amplified by a larger gain, relaxing the design of the ADC. To further reduce the noise of the CG and IDAC, dynamic element matching (DEM) is used to modulate the low-frequency noise of the CG and IDAC devices to out of band frequency [10]. More importantly, as the CG and IDAC are biased with the same IREF, the low-frequency noise contribution of IREF, which is not reduced by DEM, is suppressed in a ratiometric manner, due to the residual low-frequency noises of CG and IDAC are highly correlated.

Table IV summarizes and benchmarks the state-of-the-art BioZ readout channels. Thanks to the use of the digital-assisted baseline cancellation, the BioZ channel [66] achieves the widest input range and the best resolution compared to the others [10][16].

IV. Optical Readout Channel

Photoplethysmogram (PPG) and near-infrared spectroscopy (NIRS) are widely used optical monitoring techniques in wearable sensors [67]. Both modalities measure the blood volume change or blood chromophore change (e.g. oxy-hemoglobin and deoxy-hemoglobin) by illuminating light with one or more wavelengths into tissues and then measure the reflected/transmitted light with detectors [68][69]. The changes in light absorption can be measured (Fig. 9 (a)), and several physiological parameters can be extracted, e.g. heartbeat can be detected by a single-channel PPG signal with the light

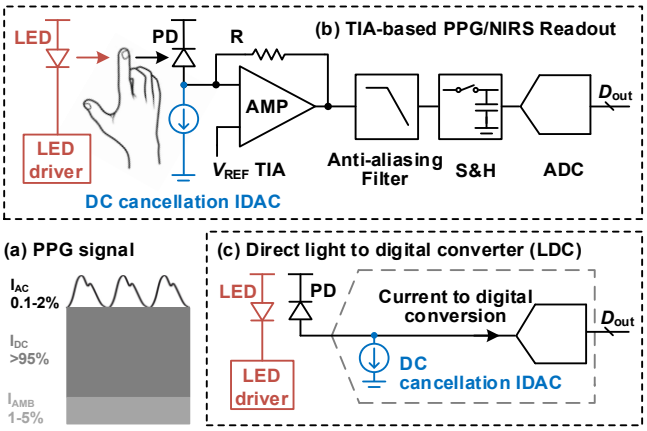

Fig. 9. (a) Reflective finger PPG/NIRS measurement and a typical PPG /NIRS signal (b) Conventional TIA-based readout (c) The LDC readout

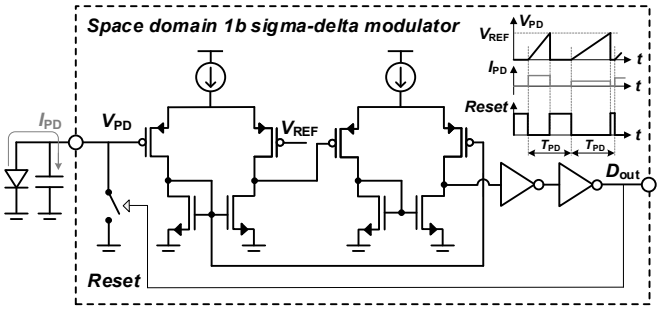

Fig. 10. Low power monolithic 1b delta-sigma LDC [27]

wavelength at visible region or NIR region, the oxygen saturation (SpO_2) can be obtained by two-channel PPG signals with NIR lights and respiration rate can be obtained if measured on the chest [70][71]. With the similar detection technique, a NIRS signal can measure the hemodynamics in the brain or the microvascular blood flow of muscle because light at NIR band (780nm-2500nm) can penetrate deeper in human tissues than light in visible band, enabling applications like brain mapping, and brain-computer interface [72][73].

From readout circuitry point of view, there are mainly two categories. The conventional readout employs an integrator or a transimpedance amplifier (TIA) to convert the light current received by the photodetector into a voltage, followed by an ADC, where the voltage output is converted to a digital code (Fig. 9 (b)). Recently, the concept of light-to-digital converter (LDC) starts to become widespread as an alternative readout topology for PPG/NIRS. The main advantages of LDCs include a more compact system architecture, less noise and power contributors by using monolithic PD and its parasitic capacitor as a passive integrator or merging the readout amplifier and ADC an active integrator (Fig. 9 (c)). The rest of this section focus on recent development in LDCs.

A. LDC with passive integrator

In heart-beat PPG monitoring, relatively low DR is required (> 25 dB) on the AC component to ensure a ±1 bpm heart-beat accuracy [14]. A low power solution is proposed by using on-chip CMOS PD, where PD is unbiased, behaving like a passive integrator [25]. As shown in Fig. 10, instead of using an active integrator or TIA, the photocurrent is integrated on PD's parasitic capacitance, generating an open-circuit voltage V_{PD}.

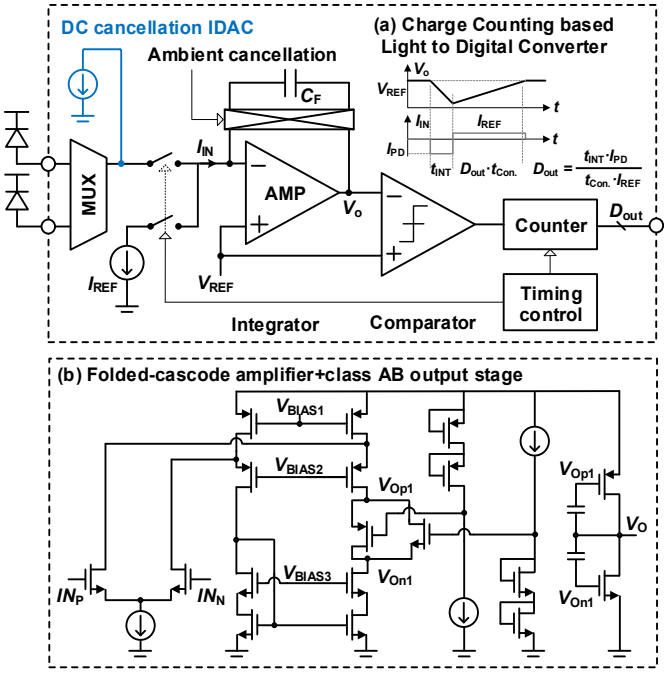

Fig. 11. (a) Dual-slope charge counting high DR LDC [77] (b) Schematic of the core amplifier

When V_{PD} is higher than the reference voltage, the comparator resets the PD and thus short pulses are generated. The time period between every two pulses is inversely proportional to the light current and thus used to obtain signal amplitude. Different from CMOS PD, another work exploits an array of on-chip pinned PDs to be the passive integrator. The pinned PDs integrate the photocurrent [26] with a unique conversion strategy. The open-circuit voltages of pinned PDs are averaged passively and then amplified by an SC amplifier, then an incremental ADC is employed to read out the averaged open-circuit voltage.

Both works are reported to have >10X power efficiency compared with TIA-based solutions. This significant reduction of power is achieved by using PD to be the passive integrator, where the current to voltage conversion takes place on PD's parasitic capacitors instead of a power-hungry transimpedance amplifier. Moreover, the LED can be pulsed with ultra-low duty-cycle because of the fast response of the small PD cells with low capacitance, thus, the LED power can be further reduced, e.g. the LED only consumes 2.63µW with a duty-cycle of 0.07% [26]. However, since the PD's parasitic capacitance changes exponentially with its open-circuit voltage, these LDC may suffer from linearity problem [74][75].

B. LDC with active integrator

In chest PPG monitoring or NIRS brain mapping, a > 100 dB DR is required due to the small perfusion index (AC/DC ratio) of the chest PPG or brain NIRS signal [76]. Another LDC architecture is proposed rather than using passive integrator but applying an active one. (Fig. 11(a)(b)) [77]. The PD is biased with a fixed voltage for better sensitivity and linearity. This active integrator is used for both current to voltage conversion and part of data conversion. The pulsed light current with a fixed pulse width firstly gets integrated on the feedback capacitor C_f, which determines the transimpedance gain to convert the light current into a voltage. At the same time, this pulsed current integration forms a low-pass function to filter out high-frequency noise. During the conversion, a reference current is applied to discharge C_f to the reference voltage, and the total discharging time is counted which represents the input light current. The time-domain conversion can ensure good linearity. DC compensation and ambient light canceling are applied for a higher dynamic range.

Table V PPG/NIRS readout comparison table

	[14]	[25]	[26]	[78]	[77]
Technology	0.13µm	0.18µm	0.18µm	0.18µm	0.18µm
VDD	1.5/2.7	--	1.8/3.3	1/2.5	1.2/3.3
Amb.Remove	6µA	--	--	28.2µA	50µA
DC.Substract	6-bit	--	--	8-bit	7-bit
PRF	100Hz	160kHz	40Hz	100Hz	512Hz
Max DR	95dB	--	--	92.7dB	119dB
LED Current @Duty Cycle	12mA @1%	--	Sub-mA @0.07%	7.6mA @10.24%	5mA @1%
LED power	0.32mW*	--	1.97µW	1.95mW	107µW
AFE Power	69 µW	13-25µW	2.63µW	8.1µW	89µW
Architecture	TIA+ADC	LDC	--	LDC	LDC

*for a 2.7V supply

This work shows a higher DR compared to TIA-based solutions. As the conventional solution needs a separated TIA, sample & hold, ADC to finish the light to digital conversion. This LDC benefits from the multi-function integrator which has less noise and power contributors. Also, the time domain counting mechanism can bring in good linearity. However, this dedicated active integrator design consumes > 10X AFE power compared with LDCs with passive integrator. [78] Exploits a current domain first order ΣΔ LDC architecture, which also applies an active integrator followed by the PD. This front-end achieving a 92.7 dB DR with only 8.1 µW. However, in order to have sufficient oversampling ratio on the same LED pulse, a wider pulse-width has to be used.

Table V summarizes the performance of the state-of-the-art PPG/NIRS readout channels. As the conclusion, compared with conventional TIA-based optical readout for PPG/NIRS applications, the LDC architectures can potentially have lower power consumption by using the PD to be a passive integrator. Also, the LDC can potentially achieve higher DR by applying an active integrator to do both amplification and part of data conversion.

V. Non-contact, capacitively-coupled technologies

This section focuses on the method of acquiring bio-signals in a capacitively-coupled manner, namely ECG and BioZ. Unlike standard contact-based technologies, the capacitively-coupled acquisition of bio-signals does not require a galvanic contact with the skin, and hence enables a 'cable-free' solution that allows performing comfortable long-term monitoring.

A. Non-contact ECG monitoring

Capacitively-coupled ECG (ccECG) was first demonstrated in 1967 [79], but it is only recently that it has gained more attention and new solutions have been developed. The main challenges of such unobtrusive measurement are: The high ETI [80][81] (up to ~4 GΩ at 10 Hz and ~60 GΩ at 0.67 Hz for through-clothing measurements); the imbalance of ETI between electrodes [81][82]; the uncontrolled ETI variations

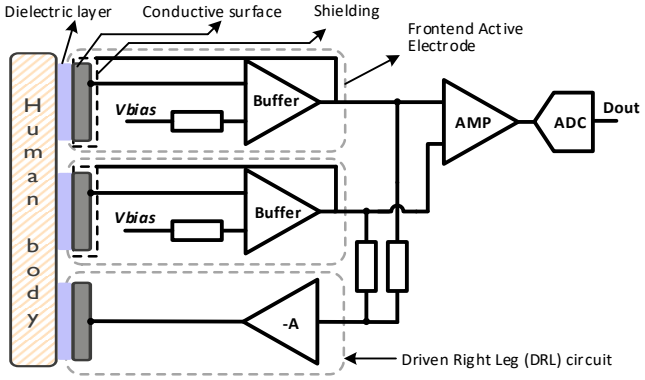

Fig. 12. General structure of a non-contact ECG acquisition circuit with Driven Right Leg feedback.

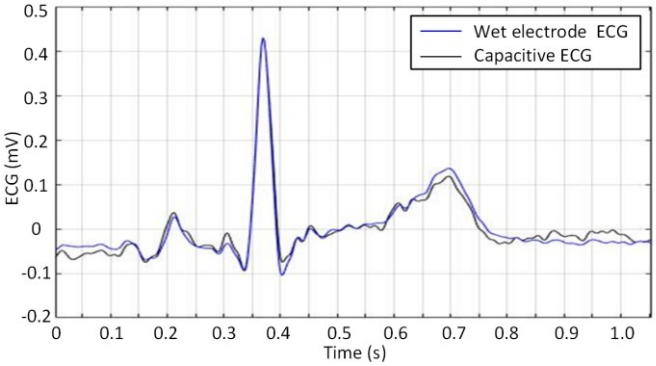

Fig. 13. Comparison between through-clothing ccECG (one layer, cotton) and medical-grade contact ECG. Achieved correlation between the signals is of 98%. ccECG amplitude scaled for ease of comparison.

[80][83]; the static charges caused by friction [83][84]; and the varying electrode coupling for different positions or body shapes when monitoring from real-life scenarios [85][86].

Coupling capacitances in ccECG can vary between a few pF when measuring through textile layers and hundreds of pF when measuring through a thin dielectric film [87]. Consequently, there is an increased impedance at the electrode interface in the frequencies of interest for ECG recording (i.e. 0.67 Hz to 40 Hz). This calls for a system using active electrodes with low input capacitance, high input resistance, low input current noise and low bias current [88]. The requirement of a high input impedance presents a tradeoff with settling time after MAs and risk of amplifier saturation [89] that needs to be taken into account.

Proposed solutions of frontend active electrodes for ccECG include the use of voltage followers with no biasing (relying on self-biasing) [87][90], using different values of resistive biasing ranging from 3 GΩ [91] to 250 GΩ [89], and more complex biasing topologies such as the use of back-to-back diodes and bootstrapping techniques [92], positive feedback techniques [93] or reset circuits [94][95].

It was concluded that a relatively simple circuit with resistive biasing allows obtaining good quality ccECG signals [80][90], and authors have shifted from complex biasing topologies [92][93] to simpler implementations [81], [90]. A tradeoff in real-life applications of a resistive bias of 50 GΩ was identified [96][97]. In addition, the use of (also non-contact) driven right leg (DRL) circuit for boosting the CMRR has been identified as necessary to obtain higher quality signals [98][99] and has become a common practice among researchers working in the field. Following this, a common structure for a ccECG acquisition circuit can be represented as shown in Fig. 12.

Application-specific integrated circuits (ASICs) for ccECG active electrodes have also been proposed, with a common goal of achieving a high input impedance and dealing with some of the main challenges in the acquisition of ccECG. These ASICs include bootstrapping techniques and on-chip biasing networks [100]-[102], positive feedback and self-calibration [103], as well as non-linear biasing together with high dynamic range (up to 220 mV_{pp}) [102] and even on-chip integrated DRL to be included in the back-end electronics [102].

Systems with commercial off-the-shelf (COTS) components have been more extensively evaluated in terms of ccECG coverage and signal quality than the recently proposed ASICs, but it is clear that these ASICs have the potential to provide a low-power and low-cost solution, given that the acquired ccECG signal in real-life scenarios is comparable to what has been obtained for the more widely studied COTS-based systems.

Regarding the performance of ccECG acquisition, it has been demonstrated that through-clothing ccECG can achieve high similarities with contact ECG [80][89]. Fig. 13 shows an example of a through-clothing (one layer, cotton) ccECG signal compared against medical-grade ECG with a correlation of 98%, acquired by the system presented in [104].

Considering the recent developments in the field, it has been identified that future innovations are likely to be at the system level rather than on circuit topologies [80], and that motion artefacts are one of the main remaining challenges [80][81][83], together with the effect of clothing thickness [105]. These system-level innovations combined with application-specific algorithms are expected to enable the use of ccECG in every-day life.

Some of the most promising system-level approaches include the use of multi-electrode arrays [104][106][107], together with signal quality indication (SQI) algorithms [108][109] to be used for real-time electrode selection [104][107] and quality-based signal post-processing [110][111]. It has been identified that an adequate channel/signal selection presents similar performance than more complex multivariate (e.g. ICA) processing techniques [112][113] and that MA compensation approaches are effective only in controlled or lab conditions, but less useful in realistic scenarios [88][114]-[115].

An additional improvement to ccECG systems is the use of digital active electrodes. A digital frontend for ccECG combined with a multi-electrode array approach has the potential to allow the evaluation of an increased number of electrode combinations using SQI-based postprocessing. Digital frontends have been proposed in literature [92][94], but its evaluation has been limited to controlled conditions without the use of a (digital) DRL. A system with digital frontends and a digital DRL adequately integrated into application-specific prototypes is expected to further improve the capabilities of ccECG monitoring in real-life scenarios.

From the application point of view, most common evaluated real-life scenarios for integration of ccECG monitoring include driver monitoring [116][118] and sleep monitoring [110][119][120], but other scenarios such as monitoring at the office [97], from a wheelchair [121], airplane seat [122], among others are certainly of interest. High performance has been

reported when applying SQI algorithms (e.g. for driver monitoring), with beat detection sensitivities achieving values higher than 98%, HR mean absolute errors of ~1 bpm (in the highway) and ~2 bpm (in the city) and R-R interval 95th percentile error within ±27.3 ms [116]. High performance has also been reported when monitoring from bed scenarios [108][119][123].

B. Non-contact BIOZ monitoring

Through-clothing capacitively-coupled Bioz (ccBioZ) measurements have been less studied than ccECG measurements. Although BioZ has a broad range of applications including impedance cardiography (ICG), impedance pneumography (IPN) and body composition, ccBIOZ measurements have been mainly tailored to the measurement of respiratory activity (i.e. IPN) by means of a four-point configuration. ccBIOZ measurements bring an important added value when combined with ccECG to enable long-term cardiorespiratory monitoring, as ECG-derived respiration (EDR) using ccECG is more challenging than when using contact ECG [110] and hence is more commonly used within the contact-based modality [124].

One of the main challenges of a ccBIOZ measurement is the requirement of a current source with high enough output impedance and low enough parasitic capacitance (including parasitics in the electrode design/integration) at the frequency of interest to allow a constant current injection through the (increased) ETI at the electrode interface. In addition, the combination of current amplitude, voltage readout gain and voltage readout resolution needs to be adequate to capture the relatively small (0.1 Ω - 1 Ω) [125][126] impedance changes corresponding to respiration, while at the same time avoiding saturation caused by a too high current or readout gain and the effect of MAs.

From the few reported ccBIOZ measurements, most of these have been done in controlled conditions [127]-[129], with a common characteristic of using an improved Howland current source [128] or a standard voltage source [130] and with purposes of ICG or IPN acquisition. All measurements reported high sensitivity to motion, which pointed to the systems being unsuitable for their use in real-life conditions. This is likely to be caused by some of the current source and readout limitations mentioned above. A system characterization (i.e. current source and readout behavior over changing loads) was not reported to allow an analysis of the causes.

In [104], a system for simultaneous ccECG & ccBioZ-based respiration was proposed, which used an ASIC [12] for the ccBioZ measurements. Although this ASIC was originally designed for contact-based measurements and its current source was not optimized yet for ccBioZ, the system was successfully evaluated in driver monitoring applications with median respiration rate coverages of 61.3% across 5 subjects. Improvements to the current source & readout circuit, together with ccBioZ SQIs are expected to increase this performance.

It is worth mentioning the frequency-dependent challenge of the current source for ccBioZ measurements. The use of higher frequencies (e.g. from ~300 kHz to 1 MHz) translates into less (capacitive) ETI at the electrode interface than the 10 kHz – 100 kHz range typically used in contact BioZ [131]. In principle, this reduces the requirements for the current source.

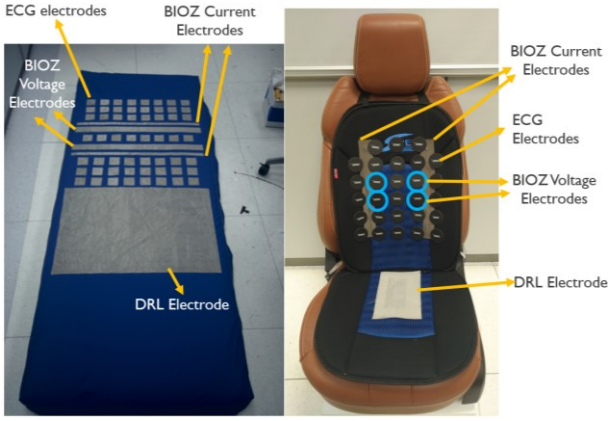

(a) (b)

Fig. 14. ccECG and ccBIOZ prototypes as example of possible integration of unobtrusive technologies in everyday life. (a) For sleep monitoring (covered by a normal bedsheet when in use). (b) For driver monitoring.

Nevertheless, there are two main drawbacks to the use of higher frequencies for ccBioZ measurements: the possibly lower effect of the physiological parameter of interest (e.g. respiratory activity) and the lower parasitic impedances that can cause a reduction in the injected current.

This calls for an evaluation of the optimal current to be used in ccBioZ measurements for specific applications under realistic conditions. Initial analysis of ccBioZ for impedance spectroscopy purposes was done in the 25 kHz – 500 kHz range in laboratory conditions measuring dummy materials [127]. This concluded that frequencies of 25 kHz and lower result in significant deviations in the measurements due to the high ETI. Nevertheless, this was not evaluated for through-clothing real-life measurements. Such an analysis focused on ccBioZ measurements in realistic scenarios, in combination with an ASIC (or COTS system) optimized for through-clothing measurements would provide a significant contribution to the field.

C. Applications of non-contact ECG & BioZ monitoring

Unobtrusively acquiring ECG and BioZ from sensors integrated into everyday life has multiple applications in healthcare. An example of possible sensor integration can be seen in Fig. 14, where a car seat and a bed are equipped with electrodes for through-clothing ccECG and ccBIOZ acquisition [104].

Extension of the time-limited Holter-based (or patch-based) ECG monitoring in cardiac patients is one of the applications, as it has been demonstrated that limited ECG monitoring time leads to missed arrhythmias [132][133]. In addition, monitoring of elderly people at home or in residential care has the potential for early identification of cardiorespiratory conditions. Identification and follow-up of sleep-related conditions such as sleep apnea in the comfort of the user's home is another important application [110][134].

Within hospital care, these unobtrusive solutions can allow performing medium-care monitoring, in situations in which this is not done due to the additional load that this would imply for hospital staff. Similarly, monitoring of infants in non-critical conditions without the burden of using glued wet or dry electrodes can be enabled both at the hospital and at home.

Behavioral-related analyses are also within the applications, ranging from stress monitoring in different scenarios (e.g. office, while driving) to the follow-up of patients with mental conditions.

Further validation of these unobtrusive signals and related algorithms in different environments\applications is required to increase the confidence of health professionals and patients/users towards unobtrusive technologies. This can be enabled by prototypes such as the ones shown in Fig. 14, together with dedicated experiments that clarify the benefit of longer, unobtrusive monitoring in everyday life.

VI. Conclusion

This paper presents an overview of the state-of-the-art multi-channel wearable SoCs, including the system architecture, three mostly used bio-signal readout channels (i.e. ExG, BioZ, PPG/NIRS) and non-contact sensing technique. Recent developments and advances are analyzed and compared with focus on circuit techniques and topologies for sensor readout. As the conclusion, there are three main aspects in the future development of multiple-modality bio-signal recording and processing SoCs: 1) higher level of integration including edge computing; 2) better performance of individual sensing channel with minimized power consumption; 3) more comfortable sensing and processing. These SoCs will boost the fast growing remote and smart healthcare devices together with big data and AI technology, further improving the health conditions of the human being.

Reference

[1] World Health Organization. “Medical devices: managing the mismatch: an outcome of the priority medical devices project.” *World Health Organization*, 2010.

[2] Webster, John G. *Design of pulse oximeters*. CRC Press, series in Medical Physics and Biomedical Engineering, 1997.

[3] Sungmee Park and S. Jayaraman, "Enhancing the quality of life through wearable technology," *IEEE Engineering in Medicine and Biology Magazine*, vol. 22, no. 3, pp. 41-48, May-June 2003.

[4] G. Wang, M. Atef and Y. Lian, "Towards a Continuous Non-Invasive Cuffless Blood Pressure Monitoring System Using PPG: Systems and Circuits Review," *IEEE Circuits and Systems Magazine*, vol. 18, no. 3, pp. 6-26, 2018.

[5] World Health Organization. "Cardiovascular diseases (CVDs) fact sheet." *World Health Organization,* 2017.

[6] A. J. Casson et al, "Wearable Electroencephalography," *IEEE Engineering in Medicine and Biology Magazine*, vol. 29, no. 3, pp. 44-56, May-June 2010.

[7] U. Ha *et al*., "A Wearable EEG-HEG-HRV Multimodal System with Simultaneous Monitoring of tES for Mental Health Management," *IEEE Transactions on Biomedical Circuits and Systems*, vol. 9, no. 6, pp. 758-766, Dec. 2015.

[8] U. Ha *et al*., "27.2 A 25.2mW EEG-NIRS multimodal SoC for accurate anesthesia depth monitoring," in *2017 IEEE International Solid-State Circuits Conference (ISSCC)*, pp. 450-451, San Francisco, CA, 2017.

[9] Villringer et al., "Near infrared spectroscopy (NIRS): a new tool to study hemodynamic changes during activation of brain function in human adults." *Neuroscience letters* 154, no. 1-2, pp. 101-104, 1993.

[10] H. Ha *et al*., "A bio-impedance readout IC with frequency sweeping from 1k-to-1MHz for electrical impedance tomography," in *2017 Symposium on VLSI Circuits*, Kyoto, pp. C174-C175, 2017.

[11] M. Kim *et al*., "21.2 A 1.4mΩ-sensitivity 94dB-dynamic-range electrical impedance tomography SoC and 48-channel Hub SoC for 3D lung ventilation monitoring system," in *2017 IEEE International Solid-State Circuits Conference (ISSCC)*, San Francisco, CA, pp. 354-355, 2017.

[12] N. Van Helleputte *et al*., "A 345 µW Multi-Sensor Biomedical SoC With Bio-Impedance, 3-Channel ECG, Motion Artifact Reduction, and Integrated DSP," *IEEE Journal of Solid-State Circuits*, vol. 50, no. 1, pp. 230-244, Jan. 2015.

[13] M. Konijnenburg *et al*., "A Multi(bio)sensor Acquisition System with Integrated Processor, Power Management, 8X LED Drivers, and Simultaneously Synchronized ECG, BIO-Z, GSR, and Two PPG Readouts," *IEEE Journal of Solid-State Circuits*, vol. 51, no. 11, pp. 2584-2595, 2016.

[14] A. Sharma *et al*., "Multi-modal smart bio-sensing SoC platform with >80dB SNR 35µA PPG RX chain," in *IEEE Symposium on VLSI Circuits (VLSI-Circuits)*, pp. 1-2, Honolulu, HI, 2016.

[15] Y. Shu *et al*., "26.1 A 4.5mm2 Multimodal Biosensing SoC for PPG, ECG, BIOZ and GSR Acquisition in Consumer Wearable Devices," *2020 IEEE International Solid- State Circuits Conference - (ISSCC)*, San Francisco, CA, USA, 2020, pp. 400-402.

[16] P. Schönle, F. Glaser, T. Burger, G. Rovere, L. Benini and Q. Huang, "A Multi-Sensor and Parallel Processing SoC for Miniaturized Medical Instrumentation," *IEEE Journal of Solid-State Circuits*, vol. 53, no. 7, pp. 2076-2087, July 2018.

[17] S. Song *et al*., "A 769 µW Battery-Powered Single-Chip SoC With BLE for Multi-Modal Vital Sign Monitoring Health Patches," *IEEE Transactions on Biomedical Circuits and Systems*, vol. 13, no. 6, pp. 1506-1517, Dec. 2019.

[18] Giacometti, Paolo, and Solomon G. Diamond. "Correspondence of electroencephalography and near-infrared spectroscopy sensitivities to the cerebral cortex using a high-density layout." *Neurophotonics* 1.2, 2014.

[19] V. Mihajlović, S. Patki and J. Xu, "Noninvasive wearable brain sensing," *2017 IEEE SENSORS*, Glasgow, pp. 1-3,2017.

[20] Werth, Jan, et al. "Unobtrusive sleep state measurements in preterm infants–A review." *Sleep medicine reviews* 32, 2017.

[21] S. Song *et al*., "A Low-Voltage Chopper-Stabilized Amplifier for Fetal ECG Monitoring With a 1.41 Power Efficiency Factor," *IEEE Transactions on Biomedical Circuits and Systems*, vol. 9, no. 2, pp. 237-247, April 2015.

[22] B. Biisze *et al*., "Ultra Low Power programmable biomedical SoC for on-body ECG and EEG processing," *2010 IEEE Asian Solid-State Circuits Conference*, Beijing, pp. 1-4, 2010.

[23] K. N. Glaros and E. M. Drakakis, "A Sub-mW Fully-Integrated Pulse Oximeter Front-End," in *IEEE Transactions on Biomedical Circuits and Systems*, vol. 7, no. 3, pp. 363-375, June 2013.

[24] J. Xu *et al*., "A 665 µW Silicon Photomultiplier-Based NIRS/EEG/EIT Monitoring ASIC for Wearable Functional Brain Imaging," in *IEEE Transactions on Biomedical Circuits and Systems*, vol. 12, no. 6, pp. 1267-1277, Dec. 2018.

[25] H. Kim and D. Jee, "A <25 µW CMOS monolithic photoplethysmographic sensor with distributed 1b delta-sigma light-to-digital convertor," in *ESSCIRC 2017 - 43rd IEEE European Solid-State Circuits Conference*, pp. 55-58, Leuven, 2017.

[26] A. Caizzone, A. Boukhayma and C. Enz, "17.8 A 2.6µW Monolithic CMOS Photoplethysmographic Sensor Operating with 2µW LED Power," in *2019 IEEE International Solid- State Circuits Conference - (ISSCC)*, pp. 290-291, San Francisco, CA, USA, 2019.

[27] M. Konijnenburg, *et al*., "A 769µW Battery-Powered Single-Chip SoC With BLE for Multi-Modal Vital Sign Health Patches," in International Solid-State Circuits Conference (ISSCC), Feb. 2019.

[28] C. J. Lukas *et al*., "A 1.02 µW Battery-Less, Continuous Sensing and Post-Processing SiP for Wearable Applications," in *IEEE Transactions on Biomedical Circuits and Systems*, vol. 13, no. 2, pp. 271-281, April 2019.

[29] H. Kino, *et al*., "Investigation of TSV Liner Interface with Multiwell Structured TSV to Suppress Noise Propagation in Mixed-Signal 3D-IC," in *IEEE Journal of the Electron Devices Society*, vol. 7, pp. 1225-1231, 2019

[30] S. Masui, K. Kanda, K. Oishi, K. Philips and H. de Groot, "An ultra-low-power wireless transceiver SoC for medical applications," *2015 IEEE International Symposium on Radio-Frequency Integration Technology (RFIT)*, pp. 1-3, Sendai, 2015.

[31] A. Ba *et al*., "A 1.3 nJ/b IEEE 802.11ah Fully-Digital Polar Transmitter for IoT Applications," *IEEE Journal of Solid-State Circuits*, vol. 51, no. 12, pp. 3103-3113, Dec. 2016.

[32] Busze, B., et al., “Ultra low power programmable biomedical SoC for on-body ECG and EEG processing,” in Proc. IEEE Asian Solid-State Circuits Conference (ASSCC), Nov. 2010, pp. 1–4.

[33] Design space exploration for scalable R-peak detection, Trading quality versus power, Michiel J. Rooijakkers, Master thesis, Eindhoven University of Technology, 2010.

[34] M. Khayatzadeh, X. Zhang, J. Tan, W. Liew and Y. Lian, "A 0.7-V 17.4 µW 3-Lead Wireless ECG SoC," in *IEEE Transactions on Biomedical Circuits and Systems*, vol. 7, no. 5, pp. 583-592, Oct. 2013.

[35] J. Portilla, G. Mujica, J. Lee and T. Riesgo, "The Extreme Edge at the Bottom of the Internet of Things: A Review," in *IEEE Sensors Journal*, vol. 19, no. 9, pp. 3179-3190, 1 May1, 2019

[36] Y. Zhang *et al*., "A Batteryless 19 µW MICS/ISM-Band Energy Harvesting Body Sensor Node SoC for ExG Applications," in *IEEE Journal of Solid-State Circuits*, vol. 48, no. 1, pp. 199-213, Jan. 2013.

[37] A. L. Mansano, Y. Li, S. Bagga and W. A. Serdijn, "An Autonomous Wireless Sensor Node with Asynchronous ECG Monitoring in 0.18 µm CMOS," in *IEEE Transactions on Biomedical Circuits and Systems*, vol. 10, no. 3, pp. 602-611, June 2016.

[38] R. Muller et al., "A Minimally Invasive 64-Channel Wireless µECoG Implant," in IEEE Journal of Solid-State Circuits, vol. 50, no. 1, pp. 344-359, Jan. 2015

[39] F. Marefat, R. Erfani, K. L. Kilgore and P. Mohseni, "26.7 A 280µW 108dB DR Readout IC with Wireless Capacitive Powering Using a Dual-Output Regulating Rectifier for Implantable PPG Recording," 2020 IEEE International Solid- State Circuits Conference - (ISSCC), San Francisco, CA, 2020, pp. 412-414

[40] R. F. Yazicioglu, P. Merken, R. Puers and C. Van Hoof, "A 60 µW 60 nV/sqrt(Hz) Readout Front-End for Portable Biopotential Acquisition Systems," IEEE Journal of Solid-State Circuits, vol. 42, no. 5, pp. 1100-1110, May 2007.

[41] M. S. J. Steyaert and W. M. C. Sansen, "A micropower low-noise monolithic instrumentation amplifier for medical purposes," in *IEEE Journal of Solid-State Circuits*, vol. 22, no. 6, pp. 1163-1168, Dec. 1987.

[42] L. Shen, N. Lu and N. Sun, "A 1-V 0.25 µW Inverter Stacking Amplifier With 1.07 Noise Efficiency Factor," *IEEE Journal of Solid-State Circuits*, vol. 53, no. 3, pp. 896-905, March 2018.

[43] S. Mondal and D. A. Hall, "A 13.9-nA ECG Amplifier Achieving 0.86/0.99 NEF/PEF Using AC-Coupled OTA-Stacking," *IEEE Journal of Solid-State Circuits*, vol. 55, no. 2, pp. 414-425, Feb. 2020.

[44] S. Wang, C. M. Lopez, M. Ballini and N. Van Helleputte, "Leakage compensation scheme for ultra-high-resistance pseudo-resistors in neural amplifiers," in *Electronics Letters*, vol. 54, no. 5, pp. 270-272.

[45] Q. Fan, F. Sebastiano, J. H. Huijsing and K. A. A. Makinwa, "A 1.8 µW 60 nV/sqrt(Hz) Capacitively-Coupled Chopper Instrumentation Amplifier in 65 nm CMOS for Wireless Sensor Nodes," *IEEE Journal of Solid-State Circuits*, vol. 46, no. 7, pp. 1534-1543, July 2011.

[46] H. Chandrakumar and D. Markovic, "27.1 A 2.8µW 80mVpp-linear-input-range 1.6GΩ-input impedance bio-signal chopper amplifier tolerant to common-mode interference up to 650mVpp," 2017 IEEE International Solid-State Circuits Conference (ISSCC), San Francisco, CA, 2017, pp. 448-449.

[47] S. Song *et al*., "A Noise Reconfigurable Current-Reuse Resistive Feedback Amplifier with Signal-Dependent Power Consumption for Fetal ECG Monitoring," *IEEE Sensors Journal*, vol. 16, no. 23, pp. 8304-8313, Dec.1, 2016.

[48] H. Jiang, S. Nihtianov and K. A. A. Makinwa, "An Energy-Efficient 3.7-nV/sqrt(Hz) Bridge Readout IC With a Stable Bridge Offset Compensation Scheme," *IEEE Journal of Solid-State Circuits*, vol. 54, no. 3, pp. 856-864, March 2019.

[49] T. Morrison, M. Nagaraju, B. Winslow, A. Bernard and B. P. Otis, "A 0.5 cm^3 Four-Channel 1.1 mW Wireless Biosignal Interface With 20 m Range," in *IEEE Transactions on Biomedical Circuits and Systems*, vol. 8, no. 1, pp. 138-147, Feb. 2014.

[50] Y. Luo, K. Teng, Y. Li, W. Mao, Y. Lian and C. Heng, "A 74-µW 11-Mb/s Wireless Vital Signs Monitoring SoC for Three-Lead ECG, Respiration Rate, and Body Temperature," in *IEEE Transactions on Biomedical Circuits and Systems*, vol. 13, no. 5, pp. 907-917, Oct. 2019

[51] J. Xu, S. Mitra, C. Van Hoof, R. F. Yazicioglu and K. A. A. Makinwa, "Active Electrodes for Wearable EEG Acquisition: Review and Electronics Design Methodology," in *IEEE Reviews in Biomedical Engineering*, vol. 10, pp. 187-198, 2017

[52] J. Xu, P. Harpe and C. Van Hoof, "An Energy-Efficient and Reconfigurable Sensor IC for Bio-Impedance Spectroscopy and ECG Recording," *IEEE Journal on Emerging and Selected Topics in Circuits and Systems*, vol. 8, no. 3, pp. 616-626, Sept. 2018.

[53] J. Xu *et al*., "A 36 µW 1.1 mm2 Reconfigurable Analog Front-End for Cardiovascular and Respiratory Signals Recording," *IEEE Transactions on Biomedical Circuits and Systems*, vol. 12, no. 4, pp. 774-783, Aug. 2018.

[54] P. Schönle *et al*., "A DC-connectable multi-channel biomedical data acquisition ASIC with mains frequency cancellation," in *2013 Proceedings of the ESSCIRC (ESSCIRC)*, Bucharest, 2013, pp. 149-152.

[55] T. Wang, L. Liu and S. Peng, "A Power-Efficient Highly Linear Reconfigurable Biopotential Sensing Amplifier Using Gate-Balanced Pseudoresistors," *IEEE Transactions on Circuits and Systems II: Express Briefs*, vol. 62, no. 2, pp. 199-203, Feb. 2015.

[56] R. Muller, S. Gambini and J. M. Rabaey, "A 0.013 mm^2 5µw, DC-Coupled Neural Signal Acquisition IC with 0.5 V Supply," in *IEEE Journal of Solid-State Circuits*, vol. 47, no. 1, pp. 232-243, Jan. 2012.

[57] S. Wang *et al*., "A Compact Quad-Shank CMOS Neural Probe With 5,120 Addressable Recording Sites and 384 Fully Differential Parallel Channels," in *IEEE Transactions on Biomedical Circuits and Systems*, vol. 13, no. 6, pp. 1625-1634, Dec. 2019.

[58] H. Kassiri *et al*., "27.3 All-wireless 64-channel 0.013mm2/ch closed-loop neurostimulator with rail-to-rail DC offset removal," *2017 IEEE International Solid-State Circuits Conference (ISSCC)*, San Francisco, CA, 2017, pp. 452-453.

[59] X. Yang *et al*., "A 108dB DR Hybrid-CTDT Direct-Digitalization ΔΣ-ΣM Front-End with 720mVpp Input Range and >300mV Offset Removal for Wearable Bio-Signal Recording," *2019 Symposium on VLSI Circuits*, Kyoto, Japan, 2019, pp. C296-C297.

[60] C. Kim, *et al*., "Sub-µVrms-Noise Sub-µW/Channel ADC-Direct Neural Recording With 200-mV/ms Transient Recovery Through Predictive Digital Autoranging," in *IEEE Journal of Solid-State Circuits*, vol. 53, no. 11, pp. 3101-3110.

[61] W. Biederman *et al*., "A 4.78 mm 2 Fully-Integrated Neuromodulation SoC Combining 64 Acquisition Channels with Digital Compression and Simultaneous Dual Stimulation," in *IEEE Journal of Solid-State Circuits*, vol. 50, no. 4, pp. 1038-1047, April 2015

[62] R. van Wegberg *et al*., "A 5-Channel Unipolar Fetal-ECG Readout IC for Patch-Based Fetal Monitoring," *IEEE Solid-State Circuits Letters*, vol. 2, no. 9, pp. 71-74, Sept. 2019.

[63] N. Van Helleputte, J. Xu, H. Ha, R. van Wegberg, S. Song, S. Stanzione, S. Zaliasl, R. van den Hoven, W. Qiu, H. Xin, C. Van Hoof and M. Konijnenburg, "Advances in biomedical sensor systems for wearable health," in *Hybrid ADCs, Smart Sensors for the IoT, and Sub-1V & Advanced Node Analog Circuit Design*, Springer, Cham, pp. 121-143, 2018.

[64] K. Kim, K. Song, K. Bong, J. Lee, K. Lee, Y. Lee, U. Ha and H.-J. Yoo, "A 24 µW 38.51 mΩrms resolution bio-impedance sensor with dual path instrumentation amplifier," in *IEEE European Solid State Circuits Conference*, Leuven, Belgium, Sep. 2017.

[65] K. Kim et al., "22.3 A 0.5V 9.26 µ W 15.28m Ω /√Hz Bio-Impedance Sensor IC with 0.55° Overall Phase Error," in *2019 IEEE International Solid- State Circuits Conference - (ISSCC)*, San Francisco, CA, USA, pp. 364-366, 2019.

[66] H. Ha et al., "A Bio-Impedance Readout IC With Digital-Assisted Baseline Cancellation for Two-Electrode Measurement," *IEEE Journal of Solid-State Circuits*, vol. 54, no. 11, pp. 2969-2979, Nov. 2019.

[67] Allen, John. "Photoplethysmography and its application in clinical physiological measurement." *Physiological measurement* 28, no. 3 pp. R1, 2007.

[68] Raichle et al. "A default mode of brain function." in *Proceedings of the National Academy of Sciences* 98, no. 2, pp. 676-682, 2001.

[69] Cui, Xu, et al. "A quantitative comparison of NIRS and fMRI across multiple cognitive tasks." *Neuroimage* 54 no. 4, pp. 2808-2821, 2011.

[70] Alian et al., "Photoplethysmography." *Best Practice & Research Clinical Anaesthesiology.* 28, no. 4, pp.395-406, 2014.

[71] Shelley, Kirk H. "Photoplethysmography: beyond the calculation of arterial oxygen saturation and heart rate." *Anesthesia & Analgesia* 105, no. 6, pp. S31-S36, 2007.

[72] Wolf, Martin et al., "Progress of near-infrared spectroscopy and topography for brain and muscle clinical applications." *Journal of biomedical optics* 12, no. 6, pp. 062104, 2007.

[73] Irani, Farzin et al., "Functional near infrared spectroscopy (fNIRS): an emerging neuroimaging technology with important applications for the study of brain disorders." *The Clinical Neuropsychologist* 21, no. 1, pp. 9-37, 2007.

[74] Tavernier, Filip, and Michiel Steyaert. "*High-speed optical receivers with integrated photodiode in nanoscale CMOS*." Springer Science & Business Media, 2011.

[75] Häberlin, Heinrich. "*Photovoltaics: system design and practice*." John Wiley & Sons, 2012.

[76] Gao, Feng, et al. "Optical tomographic mapping of cerebral hemodynamics by means of time-domain detection: methodology and phantom validation." *Physics in Medicine & Biology,* vol. 49.6, pp.1055 2004.

[77] Q. Lin *et al*., "A 196μW, Reconfigurable Light-to-Digital Converter with 119dB Dynamic Range, for Wearable PPG/NIRS Sensors," in *2019 Symposium on VLSI Circuits*, pp. C58-C59, Kyoto, Japan, 2019.

[78] F. Marefat, R. Erfani and P. Mohseni, "A 1-V 8.1- μW PPG-Recording Front-End With > 92-dB DR Using Light-to-Digital Conversion with Signal-Aware DC Subtraction and Ambient Light Removal," *IEEE Solid-State Circuits Letters*, vol. 3, pp. 17-20, 2020.

[79] P. C. Richardson, "The insulated electrode: A pasteless electrocardiographic technique," in *20th Annual conference on engineering in medicine and biology*, pp. 15–17, 1967.

[80] Y. M. Chi, T. Jung, and G. Cauwenberghs, "Dry-Contact and Noncontact Biopotential Electrodes: Methodological Review," *IEEE Rev. Biomed. Eng.*, vol. 3, pp. 106–119, 2010.

[81] Y. G. Lim, J. S. Lee, S. M. Lee, H. J. Lee, and K. S. Park, "Capacitive Measurement of ECG for Ubiquitous Healthcare," *Ann. Biomed. Eng.*, vol. 42, no. 11, pp. 2218–2227, Nov. 2014.

[82] Y. Sun and X. B. Yu, "Capacitive Biopotential Measurement for Electrophysiological Signal Acquisition: A Review," *IEEE Sens. J.*, vol. 16, no. 9, pp. 2832–2853, 2016.

[83] J. Ottenbacher and S. Heuer, "Motion Artefacts in Capacitively Coupled ECG Electrodes," *IFMBE Proc.*, vol. 25, no. 4, pp. 1059–1062, 2009.

[84] T. Wartzek, T. Lammersen, B. Eilebrecht, M. Walter, and S. Leonhardt, "Triboelectricity in Capacitive Biopotential Measurements," *IEEE Trans. Biomed. Eng.*, vol. 58, no. 5, pp. 1268–1277, May 2011.

[85] M. Czaplik *et al.*, "The Reliability and Accuracy of a Noncontact Electrocardiograph System for Screening Purposes," *Anesth. Analg.*, vol. 114, no. 2, pp. 322–327, Feb. 2012.

[86] S. Zaunseder, A. Henning, D. Wedekind, A. Trumpp, and H. Malberg, "Unobtrusive acquisition of cardiorespiratory signals," *Somnologie*, vol. 21, no. 2, pp. 93–100, Jun. 2017.

[87] E. Spinelli and M. Haberman, "Insulating electrodes: a review on biopotential front ends for dielectric skin–electrode interfaces," *Physiol. Meas.*, vol. 31, no. 10, pp. S183–S198, Oct. 2010.

[88] T. Torfs, Y. Chen, H. Kim, and R. F. Yazicioglu, "Noncontact ECG Recording System With Real Time Capacitance Measurement for Motion Artifact Reduction," *IEEE Trans. Biomed. Circuits Syst.*, vol. 8, no. 5, pp. 617–625, Oct. 2014.

[89] I. D. Castro, R. Morariu, T. Torfs, C. Van Hoof, and R. Puers, "Robust wireless capacitive ECG system with adaptive signal quality and motion artifact reduction," in *2016 IEEE International Symposium on Medical Measurements and Applications (MeMeA)*, pp. 1–6, 2016.

[90] Y. M. Chi and G. Cauwenberghs, "Wireless Non-contact EEG/ECG Electrodes for Body Sensor Networks," in *2010 International Conference on Body Sensor Networks*, pp. 297–301, 2010.

[91] Yong Gyu Lim, Ko Keun Kim, and Suk Park, "ECG measurement on a chair without conductive contact," *IEEE Trans. Biomed. Eng.*, vol. 53, no. 5, pp. 956–959, May 2006.

[92] Y. M. Chi, S. R. Deiss, and G. Cauwenberghs, "Non-contact Low Power EEG/ECG Electrode for High Density Wearable Biopotential Sensor Networks," in *2009 Sixth International Workshop on Wearable and Implantable Body Sensor Networks*, pp. 246–250, 2009.

[93] Y. M. Chi and G. Cauwenberghs, "Micropower non-contact EEG electrode with active common-mode noise suppression and input capacitance cancellation," in *2009 Annual International Conference of the IEEE Engineering in Medicine and Biology Society*, pp. 4218–4221, 2009.

[94] T. J. Sullivan, S. R. Deiss, and G. Cauwenberghs, "A Low-Noise, Non-Contact EEG/ECG Sensor," in *2007 IEEE Biomedical Circuits and Systems Conference*, pp. 154–157, 2007.

[95] E. Spinelli, M. Haberman, P. García, and F. Guerrero, "A capacitive electrode with fast recovery feature," *Physiol. Meas.*, vol. 33, no. 8, pp. 1277–1288, Aug. 2012.

[96] S. Leonhardt and A. Aleksandrowicz, "Non-contact ECG monitoring for automotive application," in 2008 5th International Summer School and Symposium on Medical Devices and Biosensors, pp. 183–185, 2008.

[97] I. D. Castro, M. Mercuri, T. Torfs, I. Lorato, R. Puers, and C. Van Hoof, "Sensor Fusion of Capacitively Coupled ECG and Continuous-Wave Doppler Radar for Improved Unobtrusive Heart Rate Measurements," IEEE J. Emerg. Sel. Top. Circuits Syst., vol. 8, no. 2, pp. 316–328, 2018.

[98] K. K. Kim, Y. K. Lim, and K. S. Park, "Common Mode Noise Cancellation for Electrically Non-Contact ECG Measurement System on a Chair," Eng. Med. Biol. Soc. 2005. IEEE-EMBS 2005. 27th Annu. Int. Conf., no. August 2015, pp. 5881–5883, 2005.

[99] K. M. Lee, S. M. Lee, K. S. Sim, K. K. Kim, and K. S. Park, "Noise reduction for non-contact electrocardiogram measurement in daily life," in Computers in Cardiology, pp. 493–496, 2009.

[100] Y. M. Chi, C. Maier, and G. Cauwenberghs, "Integrated ultra-high impedance front-end for non-contact biopotential sensing," in 2011 IEEE Biomedical Circuits and Systems Conference. *(BioCAS)*, pp. 456–459, 2011.

[101] Y. M. Chi, C. Maier, and G. Cauwenberghs, "Ultra-high input impedance, low noise integrated amplifier for noncontact biopotential sensing," IEEE J. Emerg. Sel. Top. Circuits Syst., vol. 1, no. 4, pp. 526–535, 2011.

[102] M. Chen et al., "A 400 GΩ Input-impedance Active Electrode for Non-contact Capacitively Coupled ECG Acquisition with Large Linear-Input-Range and High CM-Interference-Tolerance," IEEE Trans. Biomed. Circuits Syst., vol. 4545, no. c, pp. 1–1, 2019.

[103] J. Lee, G. H. Lee, H. Kim, and S. H. Cho, "An ultra-high input impedance analog front end using self-calibrated positive feedback," IEEE J. Solid-State Circuits, vol. 53, no. 8, pp. 2252–2262, 2018.

[104] I. D. Castro, A. Patel, T. Torfs, R. Puers, and C. Van Hoof, "Capacitive multi-electrode array with real-time electrode selection for unobtrusive ECG & BIOZ monitoring," in Eng. in Med. & Biol. Conf., EMBC, 2019.

[105] S. M. Lee, K. S. Sim, K. K. Kim, Y. G. Lim, and K. S. Park, "Thin and flexible active electrodes with shield for capacitive electrocardiogram measurement," Med. Biol. Eng. Comput., vol. 48, no. 5, pp. 447–457, May 2010.

[106] M. Oehler, V. Ling, K. Melhorn, and M. Schilling, "A multichannel portable ECG system with capacitive sensors," Physiol. Meas., vol. 29, no. 7, pp. 783–793, Jul. 2008.

[107] T. Wartzek, H. Weber, M. Walter, B. Eilebrecht, and S. Leonhardt, "Automatic electrode selection in unobtrusive capacitive ECG measurements," Proc. - IEEE Symp. Comput. Med. Syst, 2012.

[108] I. Castro et al., "Data Quality Assessment of Capacitively-coupled ECG signals," in Computers in Cardiology, pp. 4, 2019.

[109] J. Schumm, S. Axmann, B. Arnrich, and G. Tröster, "Automatic Signal Appraisal for Unobtrusive ECG Measurements," Int. J. Bioelectromagn., vol. 12, no. 4, pp. 158–163, 2010.

[110] I. D. Castro, C. Varon, T. Torfs, S. van Huffel, R. Puers, and C. van Hoof, "Evaluation of a multichannel non-contact ECG system and signal quality algorithms for sleep apnea detection and monitoring," Sensors (Switzerland), vol. 18, no. 2, pp. 1–20, 2018.

[111] B. Eilebrecht, A. Schommartz, M. Walter, T. Wartzek, M. Czaplik, and S. Leonhardt, "A capacitive ECG array with visual patient feedback," in 2010 Annual International Conference of the IEEE Engineering in Medicine and Biology, pp. 6539–6542, 2010.

[112] C. Hoog Antink, E. Breuer, D. U. Uguz, and S. Leonhardt, "Signal-Level Fusion with Convolutional Neural Networks for Capacitively Coupled ECG in the Car," Comput. Cardiol. (2010)., vol. 45, 2018.

[113] A. Serteyn, X. Lin, and O. Amft, "Reducing motion artifacts for robust QRS detection in capacitive sensor arrays," in Proceedings of the 4th International Symposium on Applied Sciences in Biomedical and Communication Technologies - ISABEL '11, pp. 1–5, 2011.

[114] G. Peng and M. F. Bocko, "Non-contact ECG employing signal compensation," in 2013 IEEE Biomedical Circuits and Systems Conference (BioCAS), pp. 57–60, 2013.

[115] A. Serteyn, R. Vullings, M. Meftah, and J. W. M. Bergmans, "Motion Artifacts in Capacitive ECG Measurements: Reducing the Combined Effect of DC Voltages and Capacitance Changes Using an Injection Signal," IEEE Trans. Biomed. Eng., vol. 62, no. 1, pp. 264–273, Jan. 2015.

[116] I. D. Castro, M. Mercuri, A. Patel, R. Puers, C. Van Hoof, and T. Torfs, "Physiological driver monitoring using capacitively coupled and radar sensors," Appl. Sci., vol. 9, no. 19, 2019.

[117] S. Leonhardt, L. Leicht, and D. Teichmann, "Unobtrusive vital sign monitoring in automotive environments—A review," Sensors (Switzerland), vol. 18, no. 9, pp. 1–38, 2018.

[118] T. Wartzek, B. Eilebrecht, J. Lem, H. J. Lindner, S. Leonhardt, and M. Walter, "ECG on the Road: Robust and Unobtrusive Estimation of Heart Rate," IEEE Trans. Biomed. Eng., vol. 58, no. 11, pp. 3112–3120, Nov. 2011.

[119] M. Takano and A. Ueno, "Noncontact In-Bed Measurements of Physiological and Behavioral Signals Using an Integrated Fabric-Sheet

Sensing Scheme," IEEE J. Biomed. Heal. Informatics, vol. 23, no. 2, pp. 618–630, 2019.

[120] H. J. Lee, S. H. Hwang, H. N. Yoon, W. K. Lee, and K. S. Park, "Heart Rate Variability Monitoring during Sleep Based on Capacitively Coupled Textile Electrodes on a Bed," Sensors, vol. 15, no. 5, pp. 11295–11311, May 2015.

[121] E. Pinheiro, O. Postolache, and P. Girao, "a Practical Approach Concerning the Capacitive Acquisition of the Electrocardiogram in a Moving Wheelchair," XX IMEKO World Congr., pp. 2–5, 2012.

[122] J. Schumm, C. Setz, M. Bächlin, M. Bächler, B. Arnrich, and G. Tröster, "Unobtrusive physiological monitoring in an airplane seat," Pers. Ubiquitous Comput., vol. 14, no. 6, pp. 541–550, Sep. 2010.

[123] M. Takano, S. Yamagishi, T. Ohmuta, Y. Fukuoka, and A. Ueno, "Non-Contact Simultaneous Measurements of Electrocardiogram and Respiratory Movements Using Capacitive Sheet Electrodes," Adv. Biomed. Eng., vol. 6, no. 0, pp. 28–36, 2017.

[124] D. Widjaja, J. Taelman, and S. Vandeput, "ECG-derived respiration: Comparison and new measures for respiratory variability," Comput. Cardiol. 2010, pp. 149–152, 2010.

[125] A. Grenvik, S. Ballou, E. McGinley, J. E. Millen, W. L. Cooley, and P. Safar, "Impedance Pneumography," Chest, vol. 62, no. 4, pp. 439–443, Oct. 1972.

[126] A. K. Gupta, "Respiration Rate Measurement Based on Impedance Pneumography," Texas Instruments, p. 11.

[127] B. Eilebrecht, J. Willkomm, A. Pohl, T. Wartzek, and S. Leonhardt, "Impedance Measurement System for Determination of Capacitive Electrode Coupling," IEEE Trans. Biomed. Circuits Syst., vol. 7, no. 5, pp. 682–689, Oct. 2013.

[128] E. Pinheiro, O. Postolache, and P. Girão, "Contactless Impedance Cardiography Using Embedded Sensors," Meas. Sci. Rev., vol. 13, no. 3, pp. 157–164, Jun. 2013.

[129] R. Macías, M. A. García, J. Ramos, R. Bragós, and M. Fernández, "Ventilation and Heart Rate Monitoring in Drivers using a Contactless Electrical Bioimpedance System," J. Phys. Conf. Ser., vol. 434, no. 1, p. 012047, Apr. 2013.

[130] P. S. Luna-Lozano and R. Pallas-Areny, "Heart Rate Detection from Impedance Plethysmography Based on Concealed Capacitive Electrodes," in XIX IMEKO World Congress, pp. 1701–1706, 2009.

[131] M. Młyńczak and G. Cybulski, "Impedance pneumography: Is it possible?," in Photonics Applications in Astronomy, Communications, Industry, and High-Energy Physics Experiments 2012, 2012, vol. 8454, pp. 84541T, May 2015.

[132] N. Dagres et al., "Influence of the duration of Holter monitoring on the detection of arrhythmia recurrences after catheter ablation of atrial fibrillation," Int. J. Cardiol., vol. 139, no. 3, pp. 305–306, Mar. 2010.

[133] S. Kinlay, "Cardiac Event Recorders Yield More Diagnoses and Are More Cost-effective than 48-Hour Holter Monitoring in Patients with Palpitations: A Controlled Clinical Trial," Ann. Intern. Med., vol. 124, no. 1_Part_1, p. 16, Jan. 1996.

[134] C. Varon, A. Caicedo, D. Testelmans, B. Buyse, and S. Van Huffel, "A Novel Algorithm for the Automatic Detection of Sleep Apnea from Single-Lead ECG," IEEE Trans. Biomed. Eng., vol. 62, no. 9, pp. 2269–2278, Sep. 2015.

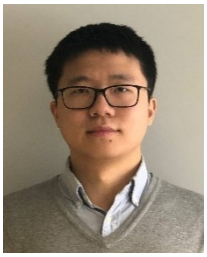

Qiuyang Lin (S'18) received the B.S. degree in electrical engineering from Dalian University of Technology, Dalian, China, in 2014, and the M.S. degree in electrical engineering from Delft University of Technology, Delft, The Netherlands, in 2016, respectively. He then joined imec, Leuven, Belgium, and Katholieke Universiteit Leuven, Leuven, Belgium, where he is currently working toward a Ph.D. degree in biomedical integrated circuit design. His research interests include biomedical readout amplifiers and data converters, low-power, low-noise, mixed-signal circuits and systems for optical sensors and other wearable biomedical applications.

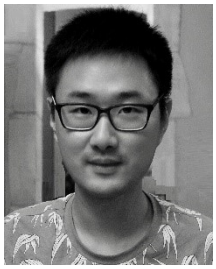

Shuang Song (S'12–M'16) received the B.S. and M.S. degree in electrical engineering from Zhejiang University, Hangzhou, China, in 2006 and 2008, respectively. He received the P.D.Eng. and Ph.D. degrees from Eindhoven University of Technology, Eindhoven, The Netherlands, in 2010 and 2015, respectively. In March 2015, he moved to Leuven, Belgium, where he is currently a Senior Researcher in connected health solutions with imec. His research interests include analog and mixed signal circuits and systems for biomedical applications, interface circuits for optical sensors and MEMS devices, data converters and low-power power management circuits. Dr. Song has authored or co-authored over 20 papers in journals and conference proceedings, he received the Anantha P. Chandrakasan Distinguished-Technical-Paper Award from ISSCC 2019.

Iván D. Castro received the degree in biomedical engineering from the Universidad Autónoma de Occidente, Cali, Colombia, in 2011 and the joint M.Sc. degree in biomedical engineering with emphasis in biomedical instrumentation from Ghent University, Ghent, Belgium and Czech Technical University, Prague, Czech Republic, in 2014. In 2019 he received his Ph.D. degree in Electrical Engineering from the University of Leuven, Leuven, Belgium, in collaboration with the Connected Health Solutions group at imec. Since 2019 he has been a researcher on health monitoring technologies and signal processing at imec. His interests include unobtrusive acquisition of biomedical signals, biomedical signal processing and digital health solutions.

Hui Jiang (S'12–M'16) received the M.E. degree in integrated circuit engineering from Tsinghua University, Beijing, China, in 2013 and the Ph.D. degree from Delft University of Technology, Delft, The Netherlands, in 2019. From 2018 to 2020, he was a researcher with imec/Holst Centre, Eindhoven, The Netherlands. In 2020, he joined the Electronic Instrumentation Laboratory, Delft University of Technology as a postdoctoral researcher. His research interests include energy efficient sensor readout ICs, high-resolution ADCs, and biomedical electronics. Dr. Jiang has authored or co-authored several patents and publications in JSSC, SSC-L, ISSCC, VLSI, CICC, ESSCIRC, and A-SSCC. He is the recipient of the ISSCC student travel grant in 2015, the third prize of the Benelux Student Chip Design Competition in 2016, and the IEEE Solid-State Circuits Society Predoctoral Achievement Award in 2018.

Mario Konijnenburg (M'08) received the M.S. degree in electrical engineering from Delft University of Technology in The Netherlands in 1993. A Ph.D. degree was received from Delft University of Technology in 1999 on Automatic Test Pattern Generation for Sequential Circuits. He joined Philips Research/NXP Semiconductors and worked on methodologies to improve design testability. Currently he is permanent member of technical staff, being system architect at imec-Netherlands Eindhoven, The Netherlands where he works on development of ultra-low power SoC designs for bio-medical applications.

Roland van Wegberg received the M.Sc. degree in electrical engineering from the Eindhoven University of Technology, Eindhoven, The Netherlands, in 1997. In 1998, he joined Philips Semiconductors/NXP as an IC Design Engineer. Since 2013, he has been a Mixed-Signal IC Design Engineer with the Analog Design Group at imec-Netherlands, where he is involved in the design of ultralow power IA, PGA, SAR-ADC, and Sigma-Delta ADCs for the amplification and digitization of biomedical signals for wearable, implantable and indigistable devices.

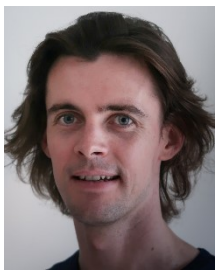

Wim Sijbers received the MS degree in electrical engineering from KU Leuven university in 2011. Since then he has been working at imec, Leuven, Belgium as an analog design engineer. Since 2017, he is part of the connected health solutions (CHS) group, imec, Leuven. His research interests include ultra-low power sensor interfaces for biomedical applications including wearable, implantable and indigistable devices.

Stefano Stanzione received the M.S. and the Ph.D. degree from the University of Pisa, Pisa, Italy, in 2006 and 2010, respectively. His Ph.D. work focused on the analog building blocks of autonomous UHF RFID tags. He joined the Holst Centre/imec, Eindhoven, The Netherlands, in 2010, where he is currently an Analog Design Engineer. His current research interests include ultra-low-power circuits for energy harvesting and battery management. Dr. Stanzione has been a member of the Analog Technical Program Sub-Committee of ISSCC between 2014 and 2018.

Dwaipayan Biswas received the M.Sc. degree in system on chip and the Ph.D. degree in electrical engineering from the University of Southampton (UoS), U.K., in 2011 and 2015, respectively. He was a Post-Doctoral Research Fellow at UoS, from 2015 to 2016. In 2016, he joined imec, Leuven, Belgium, where he has been a Researcher on digital IC design for biomedical applications. He has authored 11 journals, over 20 conference publications, and three book chapters. His research interests include low-power VLSI design, biomedical signal processing, machine learning, brain computer interface, and computer architecture.

Chris Van Hoof (M'91) received the Ph.D. degree in Electrical Engineering from the University of Leuven, Leuven, Belgium, in 1992. He is Senior Director of Connected Health Solution at imec, Leuven, Belgium and also imec Fellow. He has a track record of more than 25 years of initiating, executing, and leading national and international contract R&D with imec. His work resulted in five startups (four in the healthcare domain). His research covered highly diverse technical fields (sensors and imagers, MEMS and autonomous microsystems, wireless sensors, body-area networks, patient monitoring solutions, digital phenotyping). He has authored or co-authored more than 700 papers in journals and conference proceedings and given over 100 invited talks. He is also a Full Professor at the University of Leuven, Belgium.

Filip Tavernier (M'05) obtained the Master's degree in Electrical Engineering (ir.) and the PhD degree in Engineering Science (dr.) from Katholieke Universiteit Leuven, Leuven, Belgium, in 2005 and 2011 respectively. During 2011-2014, he was Senior Fellow in the microelectronics group at the European Organisation for Nuclear Research (CERN) in Geneva, Switzerland. During 2014-2015, he was a Postdoctoral Researcher at the Department of Electrical Engineering (ESAT-MICAS) of KU Leuven. Since October 2015, he is Assistant Professor at KU Leuven within the same department. His main research interests include circuits for optical communication, data converters, DC/DC converters and chips for extreme environments. Prof. Tavernier is member of the technical program committee of ESSCIRC and CICC and SBCCI, SSC-L Guest Editor and SSCS European Webinar Coordinator.

Nick Van Helleputte (M'07) received the MS degree in electrical engineering in 2004 from the Katholieke Universiteit Leuven, Belgium. He received his Ph.D. degree from the same institute in 2009 (MICAS research group). His PhD research focused on low-power ultra-wide-band analog front-end receivers for ranging applications. He joined imec in 2009 as an Analog R&D Design Engineer. He is currently team leader of the biomedical circuits and systems team. His research focus is on ultra-low-power circuits for biomedical applications. He has been involved in analog and mixed-signal ASIC design for wearable and implantable healthcare applications. He has authored or co-authored more than 50 papers in journals and conference proceedings. Nick is an IEEE and SSCS member and served on the technical program committee of VLSI circuits symposium and ISSCC.